Entropically modified spiking ability and periodicity in clustered channels

Jianwei Shuai,[1,*] Rong Sheng,[2] and Peter Jung[3]
[1]*Department of Physics and Institute of Theoretical Physics and Astrophysics, Xiamen University, Xiamen 361005, China*
[2]*Department of Computer Science, Sichuan University of Arts and Science, Dazhou, Sichuan 635000, China*
[3]*Department of Physics and Astronomy and Quantitative Biology Institute, Ohio University, Athens, Ohio 45701, USA*
(Received 4 November 2009; revised manuscript received 20 March 2010; published 11 May 2010)

It has been shown that, in models of excitable clusters of voltage-gated sodium channels, the spontaneous rate of action potential and signal encoding ability exhibit multiple peaks at different cluster sizes due to an entropy effect in small system. In this paper, we show that similar results can be found in excitable cluster of ligand-gated calcium channels. Furthermore, we demonstrate that the periodicity of spontaneous Ca^{2+} spikes elicited by the cluster reveals multiple maxima at small discrete cluster sizes.

DOI: 10.1103/PhysRevE.81.051913 PACS number(s): 87.16.Xa, 87.18.Hf, 87.16.Vy, 82.20.Uv

I. INTRODUCTION

It is widely known that noise can be used to enhance or induce periodicity in nonlinear nonequilibrium systems through mechanisms such as stochastic resonance [1,2]. Common to most of these studies is that noise has been added externally to subthreshold systems. At a given temperature, a certain level of intrinsic noise is always present due to the thermal fluctuations. The effects of intrinsic noise and its cellular functions have recently become a topic of interest in the study of biological systems [3–5].

In cellular systems, ionic channels change their conformations thermally and visit their open state on occasion, leading to intrinsic thermal conductance fluctuations. It is known that many channels and receptors are distributed in clusters [6–9]. For small cluster of channels, the intrinsic channel noise cannot be ignored and intrinsic stochastic resonance and coherence resonance can be found in terms of cluster size [10–13].

In the recent study of clusters of sodium channels [14,15], we showed that the rate of spontaneous action potentials and the signal encoding ability exhibit multiple maxima at small cluster sizes. A simple microcanonical theory and a combinatorial theory for the cluster entropy have been put forward to explain the multiple peaks observed in the sodium channel system.

In this paper, we show that there is a similar effect for elemental intracellular calcium signals, generated by small clusters of calcium channels. A calcium signal denotes a transient increase of intracellular calcium facilitated by the release from internal (calcium-rich) stores, most notably the endoplasmic reticulum (ER), through ligand-gated release channels, i.e., the inositol 1,4,5-trisphosphate receptors (IP_3Rs), distributed on the ER membrane [16]. Binding of extracellular agonist, such as glutamate or hormones, to metabotropic receptors generates the second messenger IP_3 which sensitizes the IP_3Rs upon binding. If cytosolic calcium binds a sensitized channel, the channel opens and calcium is released from the stores into the cytosol where it can open other channels. This leads to a rapid increase of cytosolic calcium which terminates upon channel inhibition and extrusion mechanisms. Such intracellular calcium signals regulate numerous physiologic processes in living cells [17]. For example, it has been shown that the sustained plateau IP_3 or the oscillating IP_3 concentration can produce an oscillation in cytosolic calcium [18]. The oscillation of calcium increases both the efficacy and the information content of Ca^{2+} signals that lead to gene expression and cell differentiation [19]. The Ca^{2+} oscillation with frequency at roughly physiological rates can maximize gene expression [18].

Recently, it has been shown that IP_3Rs are organized in clusters with a few or a few tens of IP_3Rs, resulting in localized Ca^{2+} release events, termed Ca^{2+} puffs or sparks [9,20–23]. These localized events are the building blocks for calcium signals on larger scales, such as cellular oscillations and waves. For the small number of channels per cluster, puffs appear stochastic with broadly distributed amplitudes and durations. The hierarchical organization of the calcium signals from stochastic puffs to intercellular waves has been in the limelight of recent investigations [23–27]. An especially interesting question is how periodicity of Ca^{2+} signals can emerge from stochastic channel dynamics. The conventional paradigm is that periodicity emerges only in the limit of large number of channels through synchronization of clusters. Here, we propose the radically different paradigm that enhanced periodicity can also occur with few channels, but only at "magic" cluster sizes.

We show here with a simple IP_3R channel model suggested by Li and Rinzel [28] that enhanced spontaneous spiking rates and signal encoding capability to weak stimuli can be found for stochastic puff releases at a discrete set of cluster sizes. Furthermore, we demonstrate that the periodicity of spontaneous Ca^{2+} spikes elicited from small clusters of IP_3Rs can be enhanced at a discrete set of cluster sizes.

II. MODEL

We now consider the model of calcium release through a small patch of an isolated ER membrane with an area of S. Assume there are N IP_3Rs distributed uniformly over the patch. The equation of continuity in conjunction leads to the

*Corresponding author. FAX: (86) 592-218-9426; jianweishuai@xmu.edu.cn

balance equation for areal cytosolic calcium concentrations C (i.e., two dimensional)

$$\frac{dC}{dt} = \frac{1}{S}\delta(z)(I_{\text{Channel}} + I_{\text{Leak}} - I_{\text{Pump}}), \tag{1}$$

where I_{Channel} describes the total current of calcium from the ER to the cytosol through all N_{Open} IP_3Rs. I_{Pump} describes calcium uptake current from the cytosol into the ER by ATP-dependent pumps. I_{Leak} describes nonspecific leak current from the ER to the cytosol. The ER membrane is located in the x-y plane.

If each IP_3R occupies an average area of S_{Channel} in the ER membrane, i.e., $S=NS_{\text{Channel}}$, and the current through a single open IP_3R is denoted by $g_{\text{Channel}}(C_{\text{ER}}-C)$, we can rewrite Eq. (1), after integrating over z, as follows

$$\frac{dC}{dt} = \frac{N_{\text{Open}}}{N} v_C (C_{\text{ER}} - C) + J_L - J_P, \tag{2}$$

with the channel flux rate $v_C=g_{\text{Channel}}/S_{\text{Channel}}$. Here, J_P and J_L describe the pump and leak flux density, respectively, with [28]

$$J_P = \frac{I_{\text{Pump}}}{S} = v_P \frac{C^2}{C^2 + k^2}, \tag{3}$$

$$J_L = \frac{I_{\text{Leak}}}{S} = v_L (C_{\text{ER}} - C), \tag{4}$$

with v_P the maximal pump flux density, v_L the leakage rate, and C_{ER} the constant concentration of calcium in ER pool.

The number of open channels is determined by using a specific model for the IP_3R. Here we use the Li-Rinzel model, in which the IP_3R has three equivalent and independent subunits [28]. Each subunit has one binding site for IP_3 and two binding sites for Ca^{2+}: one for activation and the other for inhibition. The subunit is activated if IP_3 is bound and Ca^{2+} is bound to the activating binding site. The binding rates for IP_3 and for Ca^{2+} to the activating binding site are much larger than for Ca^{2+} to the inhibiting binding site. Within a quasisteady state approximation, the fractions of subunits with IP_3 bound and Ca^{2+} bound to the activating binding site are given by

$$m_\infty = \frac{P}{P + d_m},$$

$$n_\infty = \frac{C}{C + d_n}, \tag{5}$$

respectively, where P denotes the IP_3 concentration. The binding and dissociation rates of Ca^{2+} to the inhibiting binding site are given by

$$\alpha_h = a_1 \frac{P + d_1}{P + d_2},$$

$$\beta_h = a_2 C. \tag{6}$$

The IP_3R is open only when all three subunits are activated. The fraction of open IP_3Rs is given by the product of the fraction of IP_3Rs with bound IP_3 and activating Ca^{2+}, i.e., $m_\infty^3 n_\infty^3$, and the fraction of disinhibited IP_3Rs, i.e., $(N_{\text{disinhibition}}/N)$. Hence, the channel flux density can be written as

$$J_C = v_C \left(\frac{N_{\text{disinhibition}}}{N} \right) m_\infty^3 n_\infty^3 (C_{\text{ER}} - C). \tag{7}$$

In cases where we have only few channels N, the opening and closing of the channels have to be modeled stochastically using a Markov approach [29].

In the limit of large numbers of IP_3Rs, we can use rate equation to determine the fraction of open channels. Here, the channel flux density is given by

$$J_C = v_C h^3 m_\infty^3 n_\infty^3 (C_{\text{ER}} - C), \tag{8}$$

where h satisfies the relaxation equation [28]

$$\frac{dh}{dt} = \alpha_h (1 - h) - \beta_h h. \tag{9}$$

The model parameters in Eqs. (1)–(4) and (6)–(8) are given as $v_C=80.0\ s^{-1}$, $v_P=15.0\ \mu M/s$, $v_L=0.22\ s^{-1}$, $k=0.025\ \mu M$, $C_{\text{ER}}=3.0\ \mu M$, $d_m=0.13\ \mu M$, $d_n=0.02\ \mu M$, $a_1=0.84\ s^{-1}$, $a_2=3.2\ \mu M^{-1}\ s^{-1}$, $d_1=0.13\ \mu M$, and $d_2=0.9\ \mu M$.

III. DYNAMICS OF THE DETERMINISTIC MODEL

First, we study the behavior of the model in the limit of large numbers of channels where we can use rate equation. The corresponding differential equations are solved numerically. A bifurcation diagram for C as a function of the IP_3 concentration P is shown in Fig. 1(a). A Hopf bifurcation point is found at $P=0.259\ \mu M$. We call from now on the values of P below the Hopf bifurcation the subthreshold values.

For a given subthreshold value of P, we perturb h by increasing it instantly from its steady state h_S to a larger value $h_S+\delta h$. For a perturbation larger than a threshold δh_{Min}, a spike will be elicited. Corresponding to such a threshold, there is a minimal fraction of disinhibited channels $\rho_{\text{Min}}=(h_S+\delta h_{\text{Min}})^3$ to trigger a spike. The minimal fraction ρ_{Min} is plotted as a function of P in Fig. 1(b). The figure suggests that spikes can be elicited for $P \geq 0.17\ \mu M$.

IV. MAGIC CLUSTER SIZES IN SUBTHRESHOLD REGION

Since the fluctuations of the fraction of open channels, i.e., $N_{\text{disinhibition}}/N$, is of the order $1/N$, conductance fluctuations increase with decreasing number of channels. For small numbers of channels, therefore, the rate equations used above are not viable and have to be replaced by a stochastic simulation of the opening and closing of the IP_3Rs (see [29]). As a result, the initiation of calcium signals is stochastic. As an example, we show the calcium concentration and the number of disinhibited IP_3Rs for a cluster of five IP_3Rs at the subthreshold IP_3 concentration of $P=0.2\ \mu M$ (see Fig. 2).

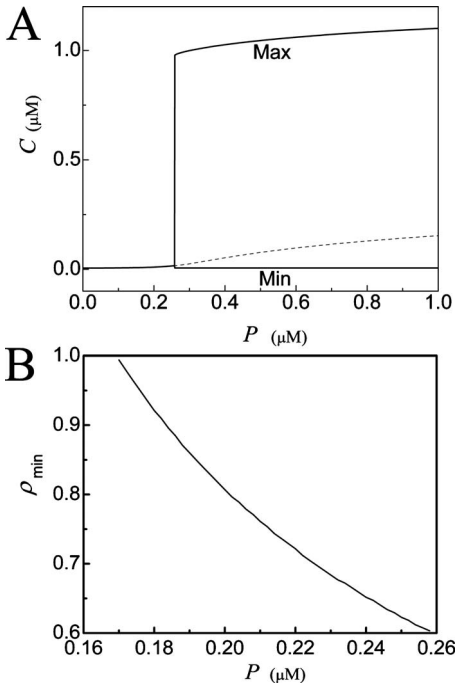

FIG. 1. Dynamics of the deterministic Li-Rinzel model. (a) Bifurcation diagram for C as a function of P. (b) Minimal h-open fraction ρ_{Min} which is necessary to trigger a spike as a function of subthreshold P.

One can see that stochastic spikes occur when $N_{\mathrm{disinhibition}} \geq 4$.

The spiking rate γ is plotted as a function of the number of channels N in Fig. 3(a) at $P=0.2$ μM. One can observe peaks of the spiking rate at multiple cluster sizes.

A simple explanation for the peaks has been suggested for subthreshold P [14]. In order to trigger a spike, the fraction of disinhibited channels must exceed ρ_{Min}. Thus, of the N channels in the cluster, there should be at least $\rho_{\mathrm{Min}}N$ channels disinhibited in order to elicit a spike. As an example, for a cluster with $N=5$ channels at $P=0.2$ μM, we find $\rho_{\mathrm{Min}}=0.798$ [Fig. 1(b)] and $\rho_{\mathrm{Min}}N=3.99$. Hence, there are two microstates, i.e., four and five disinhibited channels, related to the spiking state among a total of six microstates (i.e., 0, 1,…, 5 disinhibited channels) (Fig. 2). In general, for a cluster of N channels with $N+1$ disinhibited microstates, there are

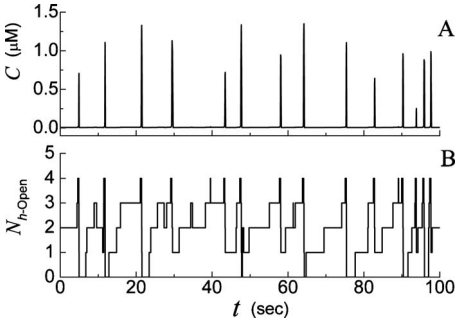

FIG. 2. (a) Calcium concentration and (b) number of disinhibited IP_3Rs for a cluster of five IP_3Rs at the subthreshold IP_3 concentration of $P=0.2$ μM.

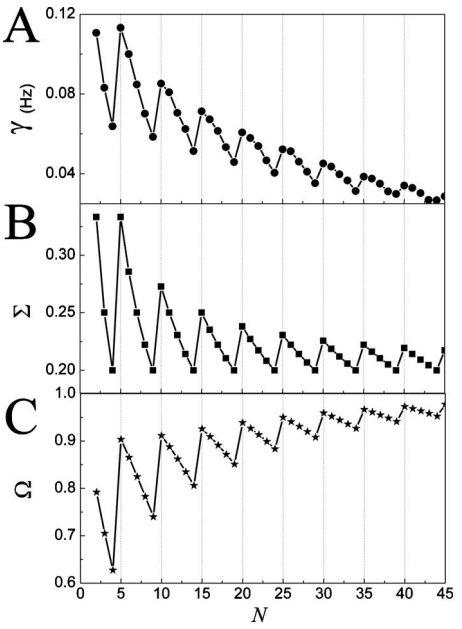

FIG. 3. (a) Spiking rate γ is shown as a function of N at $P=0.2$ μM. The entropy density [Eq. (11)] and the combinatorial probability [Eq. (14)] are shown in (b) and (c), respectively, with $\rho_{\mathrm{Min}}=0.798$.

$$M(N) = \mathrm{int}(N + 1 - \rho_{\mathrm{Min}}N) \tag{10}$$

microstates associated with the firing state. Assuming that each microstate has the same chance to occur, an entropy density Σ can be defined as [14]

$$\Sigma(N) = \frac{M(N)}{N+1} = \frac{\mathrm{int}(N+1-\rho_{\mathrm{Min}}N)}{N+1}. \tag{11}$$

This entropy density is plotted in Fig. 3(b) for $\rho_{\mathrm{Min}}=0.798$ at $P=0.2$ μM.

Figures 3(a) and 3(b) show that the peaks of the entropy density Σ as a function of N coincide exactly with the peaks in the spiking rate $\gamma(N)$ up to $N=45$. For small N, the integer function $M(N)$ in the numerator of Eq. (11) increases in large steps, with plateaus in between. Therefore, the fraction $\Sigma(N)$ of the integer function $M(N)$ and the monotonically increasing number $N+1$ exhibits peaks at the steps of $M(N)$.

The argument presented here is of course not exact, since not all microstates have the same probability. But it suggests that the discreteness of the fractions of small integer numbers is responsible for the peaks—details of the complex channel dynamics are not relevant.

A more accurate theory has also been suggested to explain the multiple peaks of spiking rate [14]. At a given subthreshold IP_3 concentration P, the probability that $N_{\mathrm{disinhibition}}$ of N channels are disinhibited and thus the other $N-N_{\mathrm{disinhibition}}$ channel are inhibited is given by the binomial distribution

$$p_N(N_{\mathrm{disinhibition}}) = \binom{N_{\mathrm{disinhibition}}}{N} h_\infty^{N_{\mathrm{disinhibition}}}(1-h_\infty)^{N-N_{\mathrm{disinhibition}}}, \tag{12}$$

with

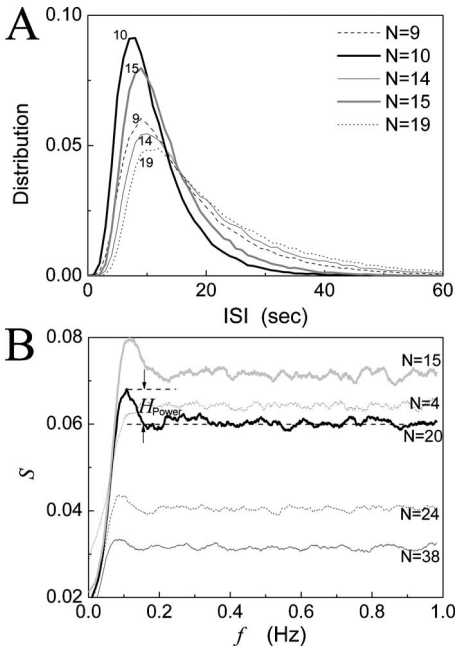

FIG. 4. (a) Interspike-interval distribution for $N=9$, 10, 14, 15, and 19 and (b) power spectra of the interspike-interval time series for $N=4$, 15, 20, 24, and 38. Here, $P=0.2$ μM

$$h_\infty = \frac{\alpha_h}{\alpha_h + \beta_h}. \tag{13}$$

According to Eq. (6), h_∞ is a function of C and P. Here we replace C by the steady-state value of the system at subthreshold P. The sum of the probabilities $p_N(N_{\text{disinhibition}})$ for all the states, in which the fractions of disinhibited channels are larger than or equal to ρ_{Min}, is defined as the combinatorial probability, i.e.,

$$\Omega = \sum_{n=N_{\text{Min}}}^{N} p_N^n, \tag{14}$$

with

$$N_{\text{Min}} = \text{int}(\rho_{\text{Min}} N) + 1. \tag{15}$$

The combinatorial probability Ω as a function of N at $P=0.2$ μM is given in Fig. 3(c). It can be seen that the combinatorial probability exhibits peaks at exactly the same system sizes as those for spiking rate and entropy density.

V. SPIKE PERIODICITY ENHANCED AT MULTIPLE CLUSTER SIZES

In this section, we study the periodicity of the calcium signals released from clustered IP_3Rs because of its importance for the cell functions [18,19]. To this end, we generate the interspike-interval distributions (ISIs), i.e., the probability densities of time intervals between two successive spikes. In Fig. 4(a), we compare the ISIs at various small cluster sizes, i.e., for $N=9$, 10, 14, 15, and 19, for a subthreshold IP_3 concentration of $P=0.2$ μM. Comparing the ISI distributions given in Fig. 4(a) to Fig. 3, it is quite striking that the distributions are narrower and more peaked for cluster sizes where the maximum spiking rates are observed. The narrower ISI distributions at $N=10$ and 15 indicate a higher temporal periodicity of the spiking signal than those at $N=9$, 14, and 19.

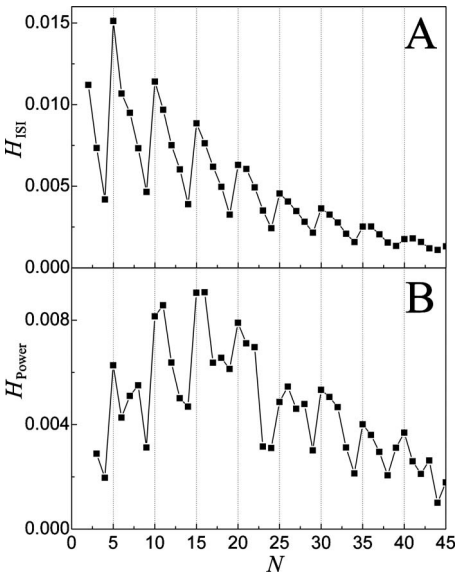

FIG. 5. Periodicity of spontaneous calcium spikes. (a) The ISI index H_{ISI} and (b) the power spectrum index H_{Power} as a function of N at $P=0.2$ μM.

In order to quantify the diversity of the ISI distribution, we define the index H_{ISI} as the ratio of the maximum and the width at half maximum amplitude. A large value of H_{ISI} indicates a narrow ISI distribution. In Fig. 5(a), the ISI index H_{ISI} is plotted as a function of N. Comparing to Fig. 3, one can see that the ISI index H_{ISI} exhibits peaks at exactly the same system sizes where the firing rates exhibit maxima (Fig. 3).

In order to verify that the decreased width of the ISIs indeed are associated with larger periodicity of the calcium signal, we calculate the power spectrum of the interspike-interval time series. The power spectrum is defined by the Fourier transform of the correlation function (see, e.g., [11])

$$S(f) = \frac{1}{T_N}\left[\left(\sum_{i=1}^{N} \sin(2\pi f T_i)\right)^2 + \left(\sum_{i=1}^{N} \cos(2\pi f T_i)\right)^2\right]. \tag{16}$$

In our simulation, 10 000 successive spikes are used to calculate the power spectrum according to above equation. The final power spectrum is averaged over 100 spike trains and then smoothed with adjacent-averaging method. The power spectra are shown in Fig. 4(b) at $N=4$, 15, 20, 24, and 38. It can be seen that a small peak is observed around $f \sim 0.1$ Hz, which indicates the appearance of a weak periodicity in ISI time series. The small peak heights in comparison to the stochastic fluctuations in the power spectrum due to a finite-length time series indicates, however, that the periodicity effect is weak.

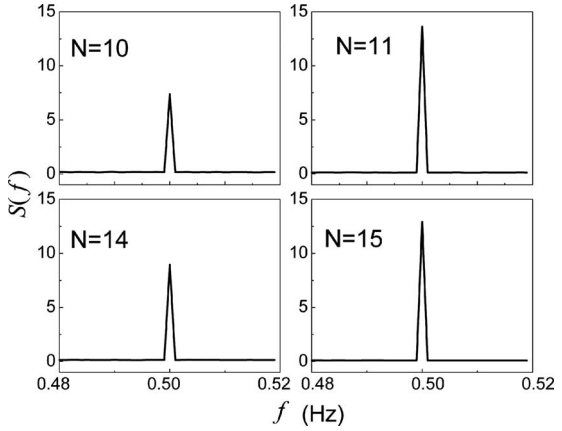

FIG. 6. Power spectra of calcium spikes responding to weak periodic IP_3 stimulus $P(t)=0.2+0.02\sin(2\pi ft)$, with $f=0.5$ Hz at $N=10$, 11, 14, and 15.

We present an index H_{Power}, which is defined as the peak height above the flat plateau, to characterize the periodicity of spontaneous Ca^{2+} spikes. In Fig. 5(b), the index H_{Power} is plotted as a function of N. Because the periodicity of spontaneous calcium spikes is weak, a rough curve for the plot of H_{Power} is obtained. Nevertheless, one can still find that the multiple peaks for H_{Power} occur at the similar cluster sizes for spiking rate given in Fig. 3. This suggests that the enhanced periodicity at multiple cluster sizes is based on the same algebraic small-number effect, distinctly different from coherence resonance found in noise-driven excitable systems [30].

VI. MULTIPLE CLUSTER SIZES FOR THE ENCODING OF WEAK SIGNALS

Binding of extracellular agonists (e.g., hormones or neurotransmitter) to metabotropic receptors in the cell membrane modulates the intracellular IP_3 concentration [18]. A larger concentration of extracellular agonist will generate more IP_3 and hence a stronger response in intracellular calcium. A small amount of agonist may not result in a cellular calcium response at all [Fig. 1(a)]. To test the dynamic response of the calcium signaling machinery to binding of agonist, we modulate the IP_3 concentration periodically and analyze the resulting calcium spikes. It is shown that the cellular response to small agonist is strongly enhanced at multiple cluster sizes equipping cells with a powerful tool to tune their calcium responses.

Stimulation by agonist is represented by a subthreshold value of IP_3 (weak stimulation) and a small periodic modulation (which is subthreshold at any time), i.e., $P(t)=0.2+0.02\sin(2\pi ft)$, with $f=0.5$ Hz. The cluster encodes the periodicity of the agonist in periodicity of spikes. Power spectra $S(f)$ of the calcium trajectories are shown in Fig. 6 for $N=10$, 11, 14, and 15. The high peaks are also observed at some cluster sizes.

A convenient measure quantifying the encoding ability of the cluster is the area of the spectral peaks around the signal frequency above the background. The signal area $A(N)$ as a function of N is shown in Fig. 7(a).

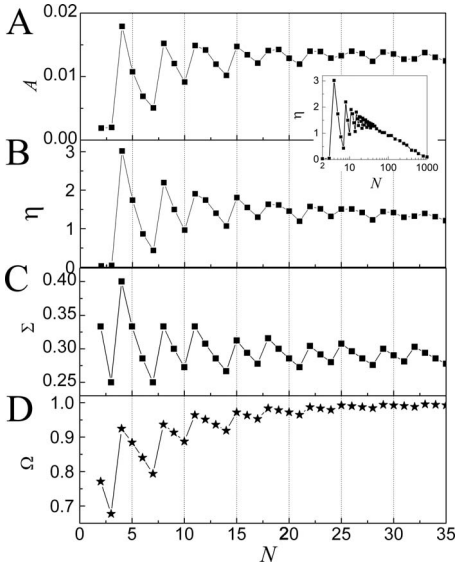

FIG. 7. Ability of the calcium signaling machinery to encode a weak periodic signal in term of (a) signal area $A(N)$ and (b) power amplification factor η. Inset shows the factor η for a larger range of system sizes N. The entropy density and the combinatorial probability are shown on (c) and (d), respectively, as a function of the system size N for $\rho_{\mathrm{Min}}=0.719$ at $P=0.22$ μM.

Because the widths and heights of the peaks in the power spectrum are determined by the length of the analyzed calcium trajectory, the area under the peak, which is independent of the length of the analyzed spike train, is of more significance. The strength of the peak in relation to the amplitude $P_1=0.02$ of the stimulus, i.e., the encoding efficiency, is characterized by the power amplification factor η [1]

$$\eta=\frac{4}{P_1^2T^2}\left|\int_0^T C_{AV}(t)\exp\left(i\frac{2\pi t}{T}\right)dt\right|^2, \tag{17}$$

with $T=1/f$ and the averaged calcium trajectory in one period

$$C_{AV}(t)=\lim_{M\to\infty}\frac{1}{M}\sum_{m=1}^{M}C(t+mT), \quad (0\le t<T). \tag{18}$$

In Fig. 7(b), we show η as a function of the cluster size N.

Both measurements of spiking periodicity shown in Figs. 7(a) and 7(b) result in the same peaks at system sizes at which the calcium signaling machinery encodes the small periodicity of the stimulus best. As shown in the inset of Fig. 7 with larger range of N, one can see clearly that the backbone of $\eta(N)$ increases for small N and then decreases for large N, exhibiting the classic stochastic resonance effect [1].

The superimposed peaks in Figs. 7(a) and 7(b) can be explained both by the entropy density and the combinatorial probability [14] as explained in the following. The spikes occur most frequently when the stimulus $P(t)$ approaches its maximum of P_0+P_1. The encoding efficiency η is thus mainly determined by the spiking rate γ at $P=P_0+P_1$. As a result, the encoding efficiency $\eta(N)$ of the cluster with N channels is related to the entropy density $\Sigma(N)$ at $\rho_{\mathrm{Min}}(P_0$

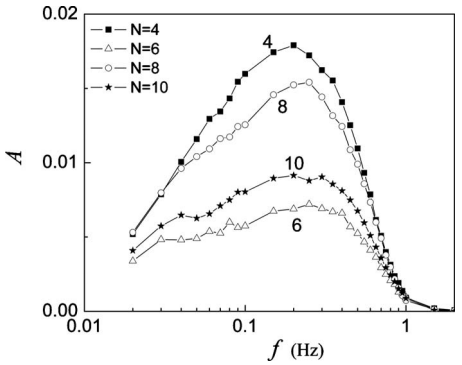

FIG. 8. Signal area $A(N)$ as a function of driving frequency f of stimulus $P(t)=0.2+0.02\sin(2\pi ft)$ at $N=4$, 6, 8, and 10.

$+P_1$). For $P_0+P_1=0.22$ μM, for example, we find $\rho_{\mathrm{Min}}=0.719$ (Fig. 1). Inserting this value into Eq. (11), we obtain the corresponding entropy density shown in Fig. 7(c). The combinatorial probability Ω as a function of N at $P=0.22$ μM with $\rho_{\mathrm{Min}}=0.719$ is also given for comparison in Fig. 7(d). For a system size of less than about $N=30$, the entropy density $\Sigma(N)$ and the combinatorial probability $\Omega(N)$ both exhibit peaks exactly where the factor $\eta(N)$ has peaks.

This discussion reveals that the peaks of encoding ability at multiple system sizes are a consequence of entropy effects in small system, a mechanism distinctly different from the stochastic multiresonance [31]. Importantly, the mechanism discussed here is not directly linked to the specific properties of the stochastic channel system. It is merely related to the small size of the clusters and properties of the arithmetic of small integers.

The encoding ability of the cluster with respect to the periodic signals also depends on the driving frequency. In Fig. 8, we show the signal area $A(N)$ as a function of driving frequency f of stimulus, i.e., $P(t)=0.2+0.02\sin(2\pi ft)$, for $N=4$, 6, 8, and 10. It can be seen that at both large and small driving frequencies, the encoding ability becomes weak. The best responding frequency is around 0.2 Hz.

VII. CONCLUSION

In this paper, we have studied a simple excitable model for calcium release from small cluster of channels. We show that channel noise can generate spontaneous spikes at a rate that exhibits peaks at multiple cluster sizes. The signaling response to a weak periodic stimulation also exhibits a similar peak structure as a function of the cluster size. Multiple peaks at various cluster sizes for spiking rate and encoding capability can be understood with a simple microcanonical theory of the cluster entropy and a more accurate combinatorial theory. Furthermore, we demonstrated by the analysis of interspike-interval distributions and power spectra that the periodicity of spontaneous spikes is enhanced at multiple cluster sizes.

We have used a very simple puff model which neglects much biological detail (such as calcium diffusion, buffers). The model focuses on the rhythmicity of spikes generated by a single cluster, which then in turn may propagate through the cell. Furthermore, we used a very simple model for the gating of the IP_3Rs. It thus remains an open problem how robust these effects are and how relevant they may be to intracellular calcium signaling.

Nevertheless, the emergence of multiple cluster sizes is a robust phenomenon that is based on a threshold and a peculiar algebraic feature of small numbers. It is largely independent on system details. It has been predicted previously for clusters of voltage-gated sodium channels for simple and complex gating models [14]. We expect that the effects described here using a very simple model will have applications for the design of sensors with engineered membrane pores or biosensors [32] that exploit the enhanced sensitivity at specific small cluster sizes.

ACKNOWLEDGMENTS

J.S. acknowledges support from the National Science Foundation of China under Grant No. 10775114 and the U.S. National Institutes of Health under Grant No. 2RO1GM065830-06A1. P.J. acknowledges support from the U.S. National Science Foundation under Grants No. IOS 0345500 and No. IOS 0744798.

[1] L. Gammaitoni, P. Hanggi, P. Jung, and F. Marchesoni, Rev. Mod. Phys. **70**, 223 (1998).
[2] L. Gammaitoni, P. Hanggi, P. Jung, and F. Marchesoni, Eur. Phys. J. B **69**, 1 (2009).
[3] H. H. Chang, M. Hemberg, M. Barahona, D. E. Ingber, and S. Huang, Nature (London) **453**, 544 (2008).
[4] C. V. Rao, D. M. Wolf, and A. P. Arkin, Nature (London) **420**, 231 (2002).
[5] G. M. Suel, R. P. Kulkarni, J. Dworkin, J. Garcia-Ojalvo, and M. B. Elowitz, Science **315**, 1716 (2007).
[6] M. B. Cannell, H. Cheng, and W. J. Lederer, Science **268**, 1045 (1995).
[7] L. Cleemann, W. Wang, and M. Morad, Proc. Natl. Acad. Sci. U.S.A. **95**, 10984 (1998).
[8] C. C. Yin and F. A. Lai, Nat. Cell Biol. **2**, 669 (2000).
[9] W. Suhara, M. Kobayashi, H. Sagara, K. Hamada, T. Goto, I. Fujimoto, K. Torimitsu, and K. Mikoshiba, Neurosci. Lett. **391**, 102 (2006).
[10] D. Bray, M. D. Levin, and C. J. Morton-Firth, Nature (London) **393**, 85 (1998).
[11] P. Jung and J. W. Shuai, EPL **56**, 29 (2001).
[12] G. Schmid, I. Goychuk, and P. Hanggi, EPL **56**, 22 (2001).
[13] J. W. Shuai and P. Jung, Phys. Rev. Lett. **88**, 068102 (2002).
[14] J. W. Shuai and P. Jung, Phys. Rev. Lett. **95**, 114501 (2005).
[15] J. W. Shuai and P. Jung, Chaos **16**, 026104 (2006).
[16] L. Ionescu, C. White, K. H. Cheung, J. Shuai, I. Parker, J. E. Pearson, J. K. Foskett, and D. O. D. Mak, J. Gen. Physiol. **130**, 631 (2007).

[17] M. J. Berridge, M. D. Bootman, and P. Lipp, Nature (London) **395**, 645 (1998).
[18] W. H. Li, J. Llopis, M. Whitney, G. Zlokarnik, and R. Y. Tsien, Nature (London) **392**, 936 (1998).
[19] R. E. Dolmetsch, K. L. Xu, and R. S. Lewis, Nature (London) **392**, 933 (1998).
[20] M. D. Bootman, M. J. Berridge, and P. Lipp, Cell **91**, 367 (1997).
[21] X. P. Sun, N. Callamaras, J. S. Marchant, and I. Parker, J. Physiol. (London) **509**, 67 (1998).
[22] T. Ur-Rahman, A. Skupin, M. Falcke, and C. W. Taylor, Nature (London) **458**, 655 (2009).
[23] S. Swillens, G. Dupont, L. Combettes, and P. Champeil, Proc. Natl. Acad. Sci. U.S.A. **96**, 13750 (1999).
[24] S. P. Dawson, J. Keizer, and J. E. Pearson, Proc. Natl. Acad. Sci. U.S.A. **96**, 6060 (1999).
[25] H. DeRemigio, M. D. LaMar, P. Kemper, and G. D. Smith, Phys. Biol. **5**, 036003 (2008).
[26] A. Skupin, H. Kettenmann, U. Winkler, M. Wartenberg, H. Sauer, S. C. Tovey, C. W. Taylor, and M. Falcke, Biophys. J. **94**, 2404 (2008).
[27] R. Thul and M. Falcke, Phys. Rev. Lett. **93**, 188103 (2004).
[28] Y. X. Li and J. Rinzel, J. Theor. Biol. **166**, 461 (1994).
[29] J. W. Shuai and P. Jung, Biophys. J. **83**, 87 (2002).
[30] A. S. Pikovsky and J. Kurths, Phys. Rev. Lett. **78**, 775 (1997).
[31] J. M. G. Vilar and J. M. Rubi, Phys. Rev. Lett. **78**, 2882 (1997).
[32] H. Bayley and P. S. Cremer, Nature (London) **413**, 226 (2001).